ASME Journal of Fluids Engineering
Online journal at:
https://asmedigitalcollection.asme.org/fluidsengineering

Xiang I. A. Yang
Department of Mechanical Engineering,
Pennsylvania State University,
University Park, PA 16802
e-mail: xzy48@psu.edu

Wen Zhang
Guangdong Provincial Key Laboratory of
Turbulence Research and Applications,
Southern University of Science and Technology,
Shenzhen 518055, China
e-mail: zhangw6@sustech.edu.cn

Junlin Yuan
Department of Mechanical Engineering,
Michigan State University,
East Lansing, MI 48824
e-mail: junlin@egr.msu.edu

Robert F. Kunz
Department of Mechanical Engineering,
Pennsylvania State University,
University Park, PA 16802
e-mail: rfk102@psu.edu

In Search of a Universal Rough Wall Model

This work compares various existing rough-wall models on a large collection of rough surfaces with different characteristics and studies the potential of these models in accommodating new datasets. We consider three empirical roughness correlations, two physics-based models, and one data-driven machine-learning model on 68 rough surfaces inside and outside the Roughness Database[1]. Results show that correlation-type models and machine-learning models do not extrapolate outside the dataset against which they are calibrated or trained. In contrast, the physics-based sheltering model performs well in extrapolation. Recalibrating a roughness correlation against a large dataset proves unfruitful. However, retraining a machine learning model yields good results. We do not pursue further retraining and recalibrating of a physics-based model, as it requires new physical insights. Overall, our findings suggest that a universal rough-wall model is yet to be found. The capability of extrapolation will likely come from incorporating physics. Data, on the other hand, benefits machine learning models. [DOI: 10.1115/1.4062820]

1 Introduction

Roughness is common in nature and in fluid engineering: barnacles on ship surfaces [1,2] and canopies in the atmospheric boundary layer [3] are examples of surface roughness. They inflict a drag penalty on the fluid flow; predicting that drag penalty is one objective of rough-wall modeling. Early work on rough-wall modeling dates back to Nikuradse [4] and Colebrook [5]. Since then, rough-wall modeling has received sustained attention [6–10]. The most commonly employed rough-wall model in fluid engineering is the Moody diagram [11]. The diagram relates the pressure drop in a pipe, i.e., a measure of the drag force, to the sandgrain roughness height and the Reynolds number. Despite its extensive use, the Moody diagram suffers from the following two inadequacies. Firstly, it is not very accurate in the transitionally rough regime [12,13]. Secondly, it requires knowledge of the equivalent sandgrain roughness height, k_s, which is often not known a priori. In fact, the primary objective of rough-wall modeling is to predict k_s based on roughness topology. In the following section, we elaborate on the problem of rough-wall modeling in Sec. 2.1, review the existing rough-wall models in Sec. 2.2, summarize the rough surfaces in the recently established roughness database in Sec. 2.3, and discuss the objective of the present work in Sec. 2.4.

2 Background

2.1 The Rough-Wall Modeling Problem. Most existing rough-wall models assume fully rough turbulent flows. The premise of rough-wall modeling is the logarithmic law [14–16]

$$U^+ = \kappa^{-1}\ln(y^+ - d^+) + B - \Delta U^+ \tag{1}$$

where U is the mean flow velocity, the superscript $+$ denotes normalization by wall units, y is the wall-normal coordinate, d is the zero-plane displacement height (often neglected,) $\kappa \approx 0.4$ is the von Kármán constant, $B \approx 5$ is the log-law intercept in the smooth-wall flow counterpart, and ΔU^+ is the roughness function [17,18]. $\Delta U^+ = 0$ for a flat-plate boundary layer, and is a logarithmic function of k_s^+ in the fully-rough regime. Equation (1) can be rewritten as

$$U^+ = \kappa^{-1}\ln\left[(y-d)/k_s\right] + A \tag{2}$$

or

$$U^+ = \kappa^{-1}\ln\left[(y-d)/y_0\right] \tag{3}$$

Here, k_s is the equivalent sand-grain roughness height; it is related to ΔU^+ as

$$\Delta U^+ = \kappa^{-1}\ln(k_s{}^+) + B - A \tag{4}$$

and $A = 8.5$ is a constant; y_0 is the equivalent roughness height, and it is related to k_s as

Contributed by the Fluids Engineering Division of ASME for publication in the Journal of Fluids Engineering. Manuscript received February 18, 2023; final manuscript received June 9, 2023; published online July 14, 2023. Assoc. Editor: Shahab Shojaei-Zadeh.

[1] roughnessdatabase.org

$$y_0 = k_s \exp(-\kappa A) \approx k_s/30 \tag{5}$$

Hence, in the fully-rough regime, knowing ΔU^+ is equivalent to knowing k_s, and knowing k_s is equivalent to knowing y_0. The objective of rough-wall modeling is to predict ΔU^+, or equivalently, y_0 or k_s, based on roughness morphology. However, predicting ΔU^+ is nontrivial because of the infinite range of possible roughness geometries. The purpose of this work is to collect as much rough-wall data as we can, and test selected existing rough-wall models on these rough walls.

2.2 Rough-Wall Models. The existing rough-wall models can be put into three categories: correlation-type models, physics-based models, and data-driven models. In the following, we review the three modeling approaches.

Correlation-type rough-wall models map roughness statistics to the equivalent sandgrain roughness height according to

$$k_s = f(\text{roughness statistics}) \tag{6}$$

The function form f is usually heuristic and contains a number of adjustable constants. These constants are calibrated against a given dataset. Early correlations like the ones in Refs. [19–21] contain one input, e.g., the solidity, where $k_s = f(\lambda_f)$. More recent correlations contain more inputs [22], e.g., k_{rms}, k_{sk}, and ES. A lot of thought has been put into the roughness statistics required within the function f. Chung et al. argued that a good correlation must contain some measure of the height, solidity, and planar coverage of the roughness [8]. Flack and Chung reviewed the existing empirical correlations in Ref. [9]. Testing all these empirical correlations is a formidable task and does not necessarily return commensurate insight. In this work, we will test the correlations in Refs. [22–24]. These three correlations read

$$k_s/k_z = 1.07(0.67\text{Sk}^2 + 0.93\text{Sk} + 1.3)(1 - e^{-3.5\text{ES}}) \tag{7}$$

which is from Ref. [22]

$$k_s/k_{\text{rms}} = 3.41(1 + \text{Sk})^{0.61} \tag{8}$$

which is from Ref. [24], and

$$k_s/k_{\text{rms}} = \begin{cases} 2.48(1 + \text{Sk})^{2.24} & Sk > 0 \\ 2.11, & Sk = 0 \\ 2.73(1 + \text{Sk})^{-0.45} & Sk < 0 \end{cases} \tag{9}$$

which is from Ref. [23]. These correlations represent the current thinking [8] and have shown good predictive power. We will test the off-the-shelf versions of these correlations and adjust the parameters to test their potential to fit new data.

Physics-based models are motivated by physical considerations such as conservation laws, flow sheltering, and velocity scalings [25–27]. Prior knowledge is often needed for the drag coefficient as a function of roughness solidity and geometry, etc. Here, we will test the two physics-based models in Refs. [28] and [29]. The model in Ref. [29] assumes the logarithmic law and a constant stress layer. Knowledge of the roughness' drag coefficient as a function of the roughness' solidity is required. Such knowledge is usually not available for an arbitrary rough surface, which limits the applications of the model. The sheltering model in Ref. [28] invokes momentum and mass conservation, the exponential law in the roughness layer [30,31], and the log law in the outer layer. The model explicitly accounts for the sheltering among roughness elements [32]. Knowledge of the drag coefficient of an unsheltered roughness element is required—unlike the sectional drag coefficient, the drag coefficient of an isolated roughness element is usually available [33]. The two physics-based models have been tested for cuboidal roughness. We will test if they predict k_s of other types of roughness. The reader is directed to Refs. [28] and [29] for further details of the two models.

Data-driven models share the philosophy of correlation-type models. However, rather than specifying the function, data-driven models delegate that task to, e.g., an artificial neural network (ANN). We will test two versions of a data-driven rough-wall model: the deep neural network (DNN) developed in Ref. [34], which was trained on 45 rough walls, and that retrained on a larger dataset presented herein. Specifically, the number of hidden layers of the DNN (i.e., 3) was kept unchanged, while the number of neurons for each of the three layers was optimized based on the current datasets. About 392 different combinations of the number of neurons per layer were tested. For each combination, the DNN compiler was performed 1000 times with random split of training (70% of total datasets) and testing (30% of total) datasets to identify the combination that yield the lowest error among all datasets.

Table 1 shows further details of the roughness models, including the type of the model, the reference, the value ranges of the roughness statistics considered when these models were developed, the number of model parameters, whether the model is interpretable, whether the model is computationally efficient, and whether the model responds to changes in roughness arrangement. For a machine learning model that employs a neural network, the number of parameters is the number of weights and biases in the network, which is usually large.

2.3 Rough Walls. We limit ourselves to homogeneous roughness whose in-plane scales are smaller than the boundary-layer height. Large in-plane scales do not usually contribute significantly to drag and can be removed by filtering [35,36]. About 68 rough walls are considered. Most of these rough walls and their respective flow data can be found in the online Roughness Database (roughnessdatabase.org). We assume full knowledge of the roughness geometry and measure roughness statistics across the entire surface rather than on a few cuts through the surface [23,24,37]. Table 2 tabulates the roughness type, the reference, and whether the flow is experimentally measured or computed in a simulation. The bidirectional-sanded surface in Ref. [37], the grit-blasted roughness in Ref. [38], the fractal-like multiscale roughness in Ref. [39], the power-law roughness in Ref. [24], and the Gaussian roughness in

Table 1 Details of the rough wall models

Reference	Type	Range of applicability	Number of parameters	Interpretable	Responsive to arrangement
MacDonald et al. [29]	Physics-based	$0.05 < \lambda_p < 0.9$	3	Yes	Partly
Yang et al. [28]	Physics-based	$0.03 < \lambda_p < 0.4$	2	Yes	Yes
Forooghi et al. [22]	Correlation	$-0.35 < \text{Sk} < 0.68,\ 0.2 < \text{ES} < 0.89$	5	No	No
Barros et al. [24]	Correlation	$-0.03 < \text{Sk} < 0.11,\ 0.09 < \text{ES} < 0.14$	2	No	No
Flack et al. [23]	Correlation	$-0.7 < \text{Sk} < 1.51,\ 0.16 < \text{ES} < 0.74$	7	No	No
Jouybari et al. [34]	Data-driven	$-1.45 < \text{Sk} < 2.37,\ 0.068 < \text{ES} < 1.1$	521	No	No

The sheltering model by Yang et al. [28] contains two parameters: the wake expansion rate and the sectional drag coefficient of an isolated, unsheltered roughness element. The physics-based model in MacDonald [29] is partly responsive to changes in roughness arrangements because one can assign different drag coefficients to different roughness arrangements. The data-driven model is a feed-forward neural network. The many hidden layers and the weights and biases give rise to a large number of parameters.

Table 2 Rough wall details

Roughness type	References	Measurement type
Bi-directional sanded	Schultz and Flack [37]	Experiment
Cuboids	Yang et al. [28]	Simulation
Grit-blasted	Thakkar et al. [38]	Simulation
Fractal-like cuboids	Yang and Meneveau [39]	Simulation
Power-law	Barros et al. [24]	Experiment
Gaussian	Flack et al. [23]	Experiment
Multiscale cuboids	Medjnoun et al. [40]	Experiment
Truncated cones	Womack et al. [41]	Experiment
Deep (slender) rectangular	Zhang et al. [31]	Simulation

Ref. [23] are irregular roughness geometries. The cuboidal roughness in Ref. [28], LEGO-like roughness in Ref. [40], truncated cones in Ref. [41], and deep rectangular roughness in Ref. [31] are regular roughness geometries. Figure 1 shows the topology of a few rough surfaces.

Figure 2 shows the ranges of the effective slope, ES_x, and the roughness skewness, Sk, of these rough surfaces. Most rough walls are within the range $0 \leq ES_x \leq 0.5$ except for the deep rectangular roughness in Ref. [31], whose ES_x is as large as 3. Most surfaces are positively skewed with$0 \leq Sk \leq 6$, except for the grit-blasted roughness in Ref. [38], and some of the Gaussian roughness in Ref. [23], which are negatively skewed. Figure 3 shows the normalized equivalent sandgrain roughness height k_s/k_{rms} as a function of the effective slope ES and the roughness skewness Sk, where k_{rms} is the root-mean-square of the surface roughness. We see that the data covers a wide range of k_s/k_{rms} values, and, as Chuang et al. pointed out, k_s/k_{rms} is not solely determined by either ES or Sk [8].

2.4 This Work. We will test the seven models in Table 1, as they are, on the 68 rough walls in Table 2. As the datasets used to develop these models were more limited than the present test data, the models will be extrapolating. Consequently, errors larger than those reported in these studies may be expected. Next, we will recalibrate the correlation-type models and retrain the data-driven model and test how well recalibrated and retrained models fit the data. The exercise will assess the potential of the two types of models in accommodating new datasets. The two physics-based models are not altered/recalibrated. Altering a physics-based model requires new physical insights, which are not always available.

The work will provide insights into the advantages and disadvantages of the various modeling approaches. The hope is that such knowledge will point us toward a universal rough-wall model.

3 Results

We apply off-the-shelf roughness models in Sec. 2.2 to the rough wall morphologies in Sec. 2.3. The results are presented in Sec. 3.1. The correlation in Ref. [24] and the neural network in Ref. [34] are recalibrated and retrained against the rough walls of Sec. 2.3. The results of the recalibrated and retrained models are shown in Sec. 3.2. The results are presented on a log scale since it is $\log(k_s^+)$ rather than k_s^+ that appears in the mean flow scaling.

3.1 Rough-Wall Models as They Are. The predictions of the physics-based models are compared to data in Fig. 4. The model in Ref. [29] is responsive to only the roughness solidity λ_f and is agnostic to changes in roughness skewness, roughness height, or roughness arrangement. Consequently, the model predicts similar $k_{s,p}$ for a wide range of roughness whose k_s varies by almost two orders of magnitude. The sheltering model in Ref. [28] extrapolates well and returns reasonably good estimates for all types of roughness. In particular, the model responds to changes in roughness arrangements, yielding less flow sheltering and therefore larger k_s for staggered roughness and more flow sheltering and therefore

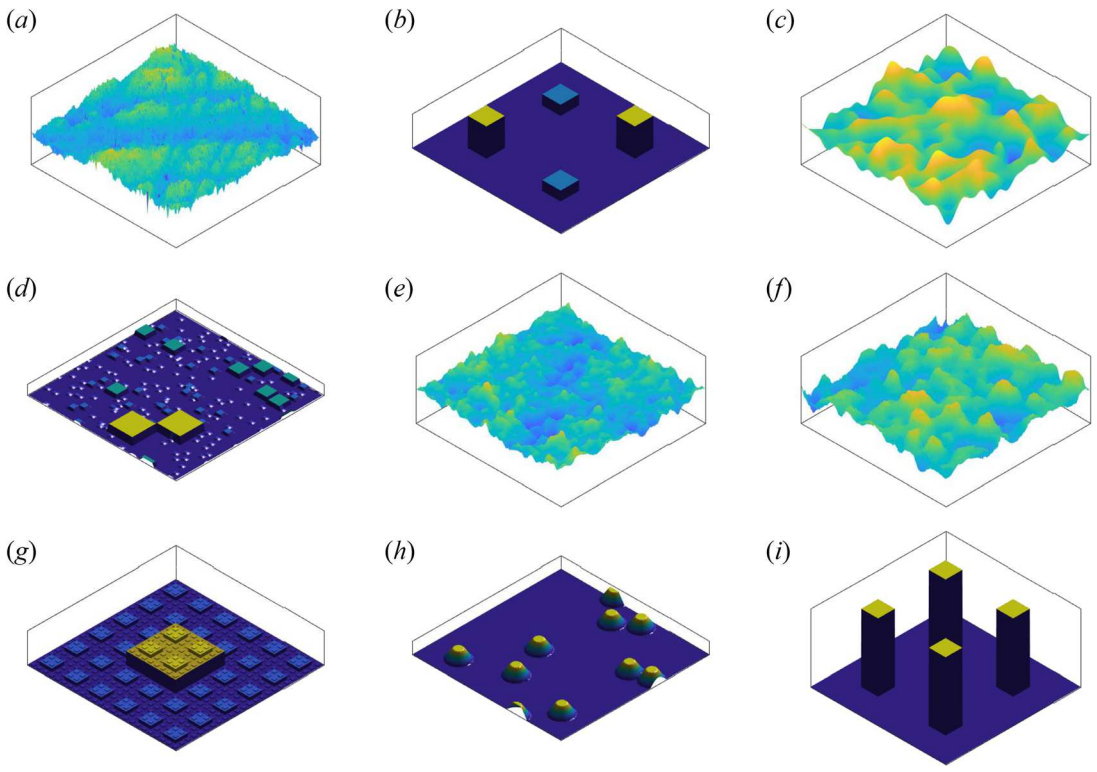

Fig. 1 Rough wall topology: (*a*) bi-directional sanded roughness in Ref. [37], (*b*) cuboidal roughness in Ref. [28], (*c*) grit-blasted roughness in Ref. [38], (*d*) fractal-like roughness in Ref. [39], (*e*) power-law roughness in Ref. [24], (*f*) Gaussian roughness in Ref. [23], (*g*) LEGO like roughness in Ref. [40], (*h*) truncated cones in Ref. [41], and (*i*) deep rectangular roughness in Ref. [31]

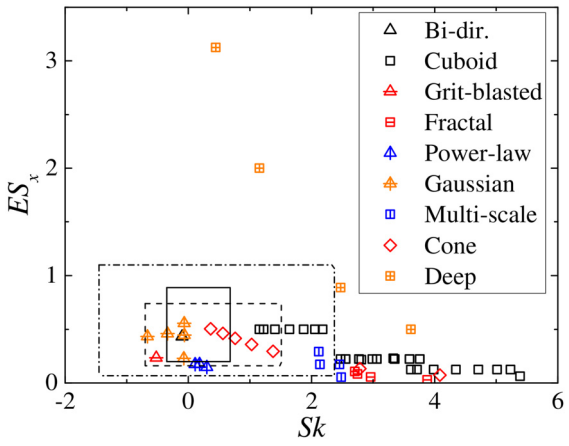

Fig. 2 Effective slope and skewness of the rough walls in Table 2. The solid, dashed, and dash-dotted squares indicate the parameter ranges used to develop the correlations in Refs. [22,23, and 34], respectively.

smaller k_s for aligned roughness. While this captures the correct physics when the roughness elements are closely packed [42], the physics is such that secondary flow arises when the roughness elements are sparsely packed [43]. These secondary flows bring high momentum fluid to within the roughness layer, leading to similar k_s for staggered and aligned roughness, which is not captured by the sheltering model. Errors are also found for multiscale roughness, for which the physics is unclear and therefore not accounted for in the model. Figure 5 shows the results for the three correlation-type models. The correlation-type models do not perform well. The k_s estimates are one to two orders of magnitude off for many of the surfaces. Lastly, Fig. 6 shows the results of the machine learning model. The model performs reasonably well. Extrapolation is still a challenge, like any other data-driven model, and there are significant errors in surfaces with multiscale roughness and cubical roughness. It is difficult to interpret the correlation models and the machine learning model, and a more detailed discussion of these results is not pursued here.

3.2 Re-Calibration and Re-Training. The correlations in Refs. [22–24] and the neural network in Ref. [34] are recalibrated and retrained against the rough walls in Sec. 2.3. First, we recalibrate the correlation in Ref. [24] against all 68 surfaces by adjusting C_1,

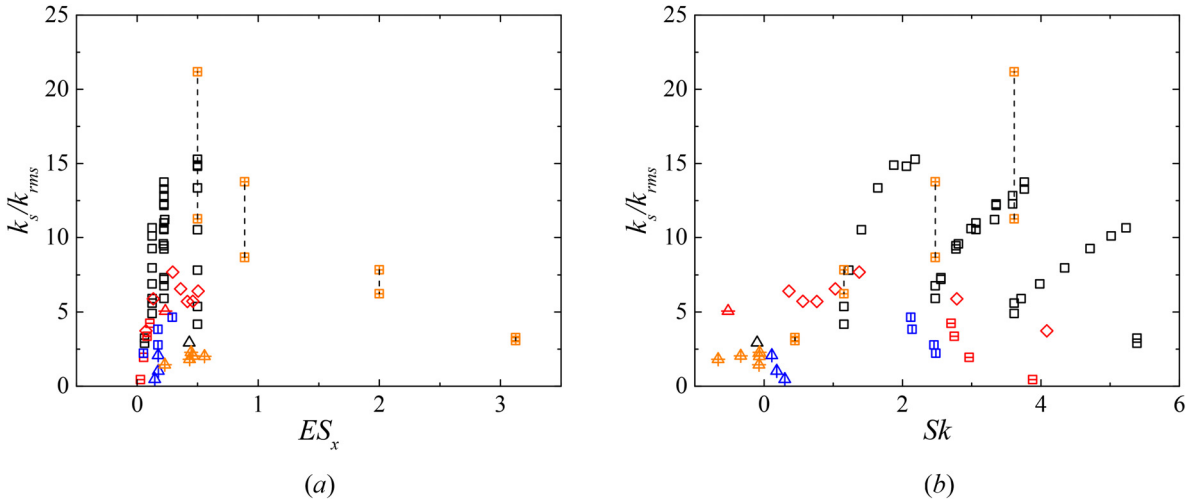

Fig. 3 k_s/k_{rms} as a function of (*a*) ES_x or (*b*) S_k for all the rough surfaces. The symbols are the same as in Fig. 2. The dashed lines connects two surfaces that are differ only in their arrangements (one is aligned, and one is staggered).

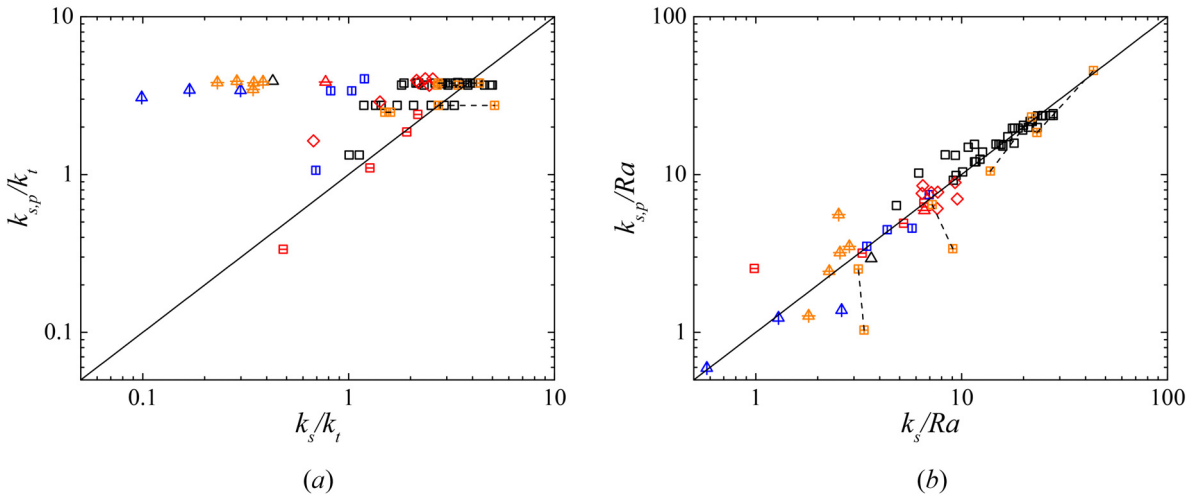

Fig. 4 Predicted k_s as a function of the measured k_s for (*a*) the model in Ref. [29] and (*b*) the model in Ref. [28]. The symbols are the same as in Fig. 2. Here, $k_{s,p}$ is the predicted equivalent sandgrain roughness height, and K_s is the data.

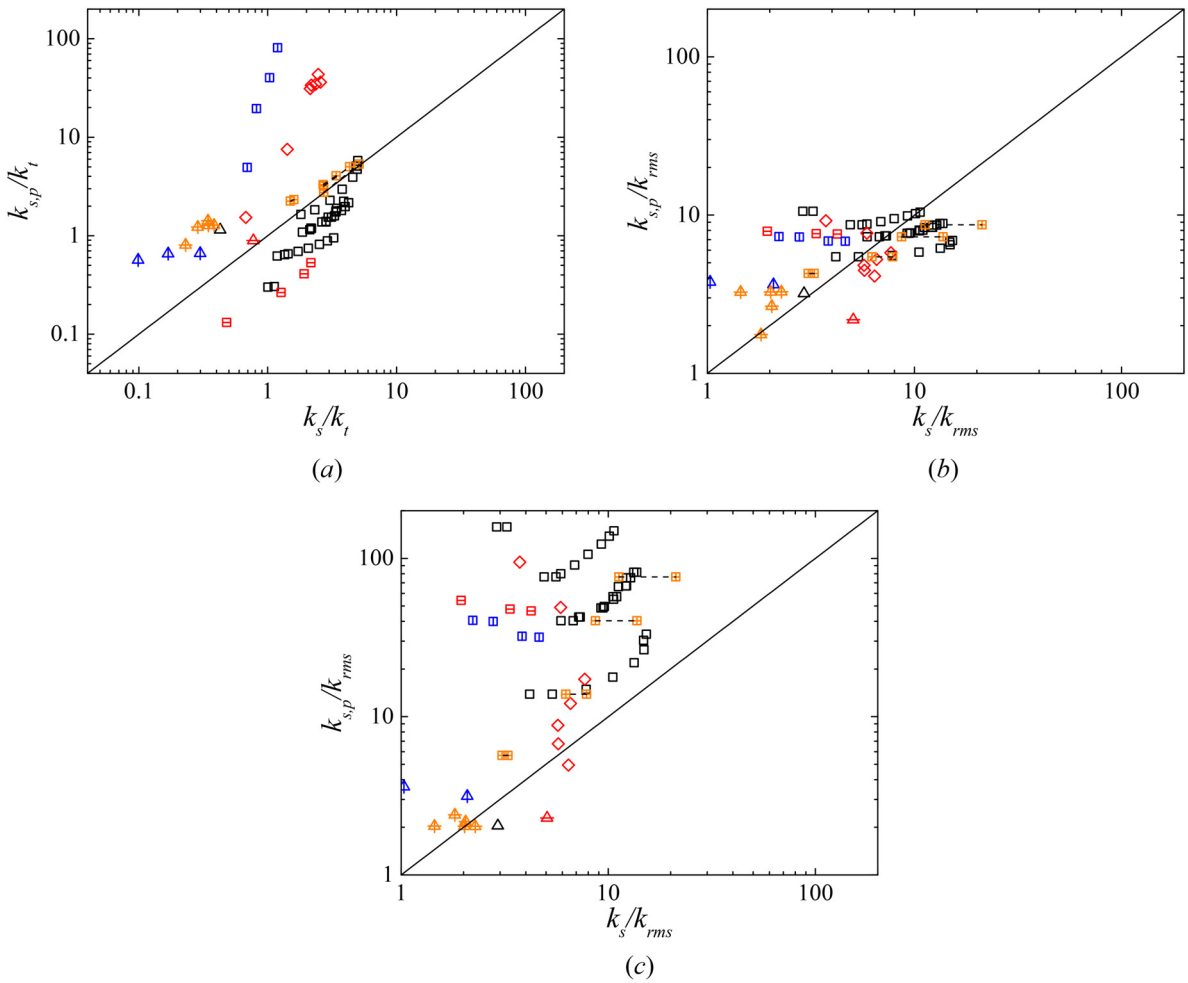

Fig. 5 Same as Fig. 4 but for (*a*) the model in Ref. [22], (*b*) the model in Ref. [24], and (*c*) the model in Ref. [23]

C_2, and C_3 in $k_{s,p}/k_{\text{rms}} = C_1(C_2 + Sk)^{C_3}$ such that the recalibrated correlation best fits the data. The results are shown in Fig. 7. Comparing Figs. 7 to 5(*b*), we see no significant improvement. This is not unexpected. The correlation contains k_{rms}, Sk, and 3 constants and therefore has very limited descriptive power. Next, we recalibrate the correlation for each type of roughness separately. Table 3 tabulates the model constants and the roughness used for recalibration. The results are shown in Fig. 8. The model constants vary drastically from one dataset to another. Nonetheless, this time, we see a close agreement between the predicted k_s and the data. Repeating the above exercise for the two correlations in Refs. [22,23] gives very similar results (not shown here for brevity.) Last, we retrain the neural network in Ref. [34] against all 68 rough surfaces. The results are shown in Fig. 9, and we see a close agreement between the network's predictions and the data without separately retraining for each type of roughness. However, this particular neural network does not capture the difference among

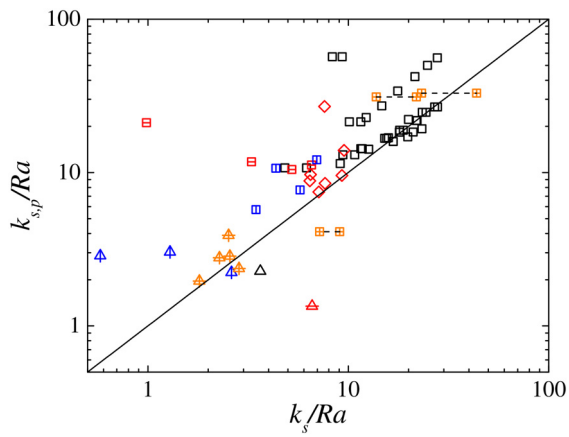

Fig. 6 Same as Fig. 4 but for the model in Ref. [34]

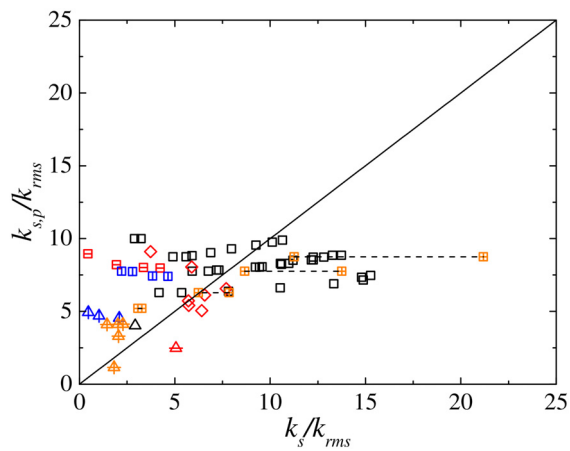

Fig. 7 Same as Fig. 5(*b*) but for the recalibrated correlation $k_{s,p}/k_{\text{rms}} = 4.96(0.68+Sk)^{0.39}$

Table 3 Roughness and the recalibrated constants

Roughness	Reference	C_1	C_2	C_3
Bi-directional sanded	Schultz and Flack [37]	3.6	0.68	0.39
Cuboids, $\lambda_p = 0.06$	Yang et al. [28]	6.9	−3	0.54
Cuboids, $\lambda_p = 0.11$	Yang et al. [28]	12	−2.4	0.31
Cuboids, $\lambda_p = 0.25$	Yang et al. [28]	15	−1.1	0.27
Gaussian cubes	Yang et al. [28]	2.2	1.0	1.1
Grit-blasted, S8	Thakkar et al. [38]	10	0.68	0.39
Fractal-like cuboids	Yang and Meneveau [39]	0.89	−2.4	−1.4
Power-law	Barros et al. [24]	4.0	1.0	6.0
Gaussian	Flack et al [23]	2.0	1.0	−0.3
Multiscale cuboids	Medjnoun et al. [40]	2.1	−2.1	−0.17
Truncated cones	Womack et al. [41]	7.5	1.0	−0.41
Deep rectangular	Zhang et al. [31]	5.2	0.15	0.85

We recalibrate against cubes of different surface coverage densities in Ref. [28] separately. "Gaussian cube" is cubes whose heights satisfy the Gaussian distribution.

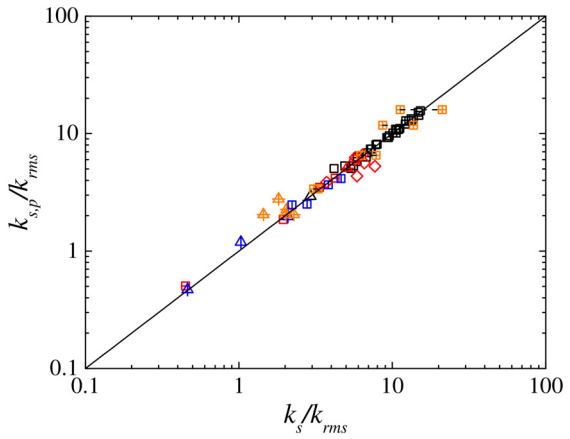

Fig. 8 Same as Fig. 4 but for the recalibrated correlation $k_{s,p}/k_{rms} = C_1(C_2+Sk)^{C_3}$. The values of the three constants are tabulated in Table 3.

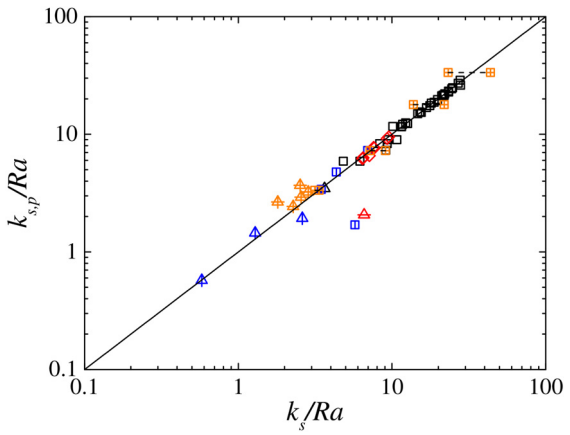

Fig. 9 Same as Fig. 4 but for the retrained neural network

cuboidal roughness with varying element arrangements, as it does not use surface inputs that describe such differences.

4 Conclusions

This work tests 7 rough wall models on 68 rough surfaces inside and outside the Roughness Database. The study covers physics-based roughness models, correlation-type models, and data-driven models. Regular and irregular roughness are considered, as well as single-scale and multiscale roughness. The off-the-shelf sheltering model in Ref. [28] works very well. Although it was originally developed for cuboidal roughness, the model gives accurate k_s estimates for most rough walls tested, responding accurately to changes in essentially all single-point roughness statistics and roughness' arrangements. However, a physics-based model is as effective as the scope of physics it incorporates; for the present models, sparse and fractal roughness may pose particular challenges. The off-the-shelf empirical correlations in Refs. [22–24] work poorly, yielding k_s estimates that are often one to two orders of magnitudes off for some correlations. The off-the-shelf machine learning model in Ref. [34] also yields significant errors for some types of roughness due to extrapolation (like any other machine learning model).

The many rough surfaces and comprehensive surface data in the Roughness Database allow for easy recalibration. We recalibrate and retrain the empirical correlation in Ref. [24] and the neural network in Ref. [34]. Retraining the correlation against all 68 rough walls yields no significant improvement. However, when the correlation is recalibrated separately for Gaussian roughness, power-law roughness, and fractal roughness, etc., it gives accurate k_s predictions. On the other hand, retraining the machine learning model against all 68 rough walls proves to be fruitful—although the retrained model does not respond to changes in roughness arrangement due to the lack of such surface features in model inputs.

We summarize our observations below. Correlation-type models are easy to implement. They give accurate predictions if calibrated against and applied to the same type of roughness. Physics-based models generalize better than correlation-type models and machine-learning models, but more data does not necessarily help improve the performance of physics-based models and, instead, missing physics needs to be identified and incorporated. On the other hand, more data directly translates to improved model performance for machine learning models. This provides an interesting possibility for rough-wall modeling: a good rough-wall model might be the result of a lot of data and limited flow physics.

Funding Data

- NSF (Grant No. 2231037; Funder ID: 10.13039/100000084).
- NSFC (Grant No. 12102168; Funder ID: 10.13039/501100001809).

Data Availability Statement

The datasets generated and supporting the findings of this article are obtainable from the corresponding author upon reasonable request.

Nomenclature

A = log law intercept
A_f = frontal area
A_p = planar area
A_t = total planar area
B = log law intercept
C_d = drag coefficient
ES = effective slope
ES_x = streamwise effective slope
ES_z = spanwise effective slope
h = surface elevation
k = roughness height
k_c = maximum peak-to-trough height
k_{rms} = root-mean-square height
k_s = equivalent sand-grain roughness height
$k_{s,p}$ = predicted equivalent sand-grain roughness height
k_t = average peak-to-trough height obtained from a surface tile of size $\delta \times \delta$
Ra = mean roughness height

Sk = skewness
Ku = kurtosis
U = mean streamwise velocity
y = wall-normal distance
y_0 = equivalent roughness height
ΔU^+ = roughness function
κ = von Kármán constant
λ_f = solidity
λ_p = planar density

References

[1] Schultz, M., Bendick, J., Holm, E., and Hertel, W., 2011, "Economic Impact of Biofouling on a Naval Surface Ship," Biofouling, **27**(1), pp. 87–98.
[2] Monty, J., Dogan, E., Hanson, R., Scardino, A., Ganapathisubramani, B., and Hutchins, N., 2016, "An Assessment of the Ship Drag Penalty Arising From Light Calcareous Tubeworm Fouling," Biofouling, **32**(4), pp. 451–464.
[3] Barlow, J. F., and Coceal, O., 2009, "A Review of Urban Roughness Sublayer Turbulence," Met Office Research and Development, Technical Report 1, p. 527.
[4] Nikuradse, J., 1950, "Laws of Flow in Rough Pipes," National Advisory Committee for Aeronautics, Washington, DC, Technical Memorandum, p. 1292.
[5] Colebrook, C. F., 1939, "Turbulent Flow in Pipes, With Particular Reference to the Transitional Region Between Smooth and Rough Wall Laws," J. Inst. Civ. Eng., **11**(4), pp. 133–156.
[6] Jimenez, J., 2004, "Turbulent Flows Over Rough Walls," Annu. Rev. Fluid Mech., **36**(1), pp. 173–196.
[7] Flack, K. A., and Schultz, M. P., 2010, "Review of Hydraulic Roughness Scales in the Fully Rough Regime," ASME J. Fluids Eng., **132**(4), p. 041203.
[8] Chung, D., Hutchins, N., Schultz, M. P., and Flack, K. A., 2021, "Predicting the Drag of Rough Surfaces," Annu. Rev. Fluid Mech., **53**(1), pp. 439–471.
[9] Flack, K. A., and Chung, D., 2022, "Important Parameters for a Predictive Model of ks for Zero Pressure Gradient Flows," AIAA Paper No. 2022-1036.
[10] Klewicki, J. C., 2010, "Reynolds Number Dependence, Scaling, and Dynamics of Turbulent Boundary Layers," ASME J. Fluids Eng., **132**(9), p. 094001.
[11] Moody, L. F., 1944, "Friction Factors for Pipe Flow," Trans. ASME, **66**(8), pp. 671–678.
[12] Allen, J., Shockling, M., and Smits, A., 2005, "Evaluation of a Universal Transitional Resistance Diagram for Pipes With Honed Surfaces," Phys. Fluids, **17**(12), p. 121702.
[13] Langelandsvik, L., Kunkel, G., and Smits, A. J., 2008, "Flow in a Commercial Steel Pipe," J. Fluid Mech., **595**, pp. 323–339.
[14] Townsend, A. A., 1976, *The Structure of Turbulent Shear Flow*, 2nd ed., Cambridge University Press, Cambridge, UK.
[15] Raupach, M., Antonia, R., and Rajagopalan, S., 1991, "Rough-Wall Turbulent Boundary Layers," ASME Appl. Mech. Rev., **44**(1), pp. 1–25.
[16] Marusic, I., Monty, J. P., Hultmark, M., and Smits, A. J., 2013, "On the Logarithmic Region in Wall Turbulence," J. Fluid Mech., **716**, p. R3.
[17] Clauser, F. H., 1954, "Turbulent Boundary Layers in Adverse Pressure Gradients," J. Aeronaut. Sci., **21**(2), pp. 91–108.
[18] Hama, F. R., 1954, "Boundary-Layer Characteristics for Smooth and Rough Surfaces," Trans. SNAME, **62**, pp. 333–351.
[19] Simpson, R. L., 1973, "A Generalized Correlation of Roughness Density Effects on the Turbulent Boundary Layer," AIAA J., **11**(2), pp. 242–244.
[20] Sigal, A., and Danberg, J. E., 1990, "New Correlation of Roughness Density Effect on the Turbulent Boundary Layer," AIAA J., **28**(3), pp. 554–556.
[21] Waigh, D. R., and K, R., 1998, "Improved Aerodynamic Characterization of Regular Three-Dimensional Roughness," AIAA J., **36**(6), pp. 1117–1119.
[22] Forooghi, P., Stroh, A., Magagnato, F., Jakirlic, S., and Frohnapfel, B., 2017, "Toward a Universal Roughness Correlation," ASME J. Fluids Eng., **139**(2), p. 121201.
[23] Flack, K. A., Schultz, M. P., and Barros, J. M., 2020, "Skin Friction Measurements of Systematically-Varied Roughness: Probing the Role of Roughness Amplitude and Skewness," Flow Turbul. Combust., **104**(2–3), pp. 317–329.
[24] Barros, J. M., Schultz, M. P., and Flack, K. A., 2018, "Measurements of Skin-Friction of Systematically Generated Surface Roughness," Int. J. Heat Fluid Flow, **72**, pp. 1–7.
[25] Harman, I., and Finnigan, J., 2007, "A Simple Unified Theory for Flow in the Canopy and Roughness Sublayer," Boundary-Layer Meteorol., **123**(2), pp. 339–363.
[26] Aupoix, B., 2016, "Revisiting the Discrete Element Method for Predictions of Flows Over Rough Surfaces," ASME J. Fluids Eng., **138**(3), p. 031205.
[27] Altland, S., Xu, H. H., Yang, X. I., and Kunz, R., 2022, "Modeling of Cube Array Roughness: Rans, Large Eddy Simulation, and Direct Numerical Simulation," ASME J. Fluids Eng., **144**(6), p. 061106.
[28] Yang, X. I. A., Sadique, J., Mittal, R., and Meneveau, C., 2016, "Exponential Roughness Layer and Analytical Model for Turbulent Boundary Layer Flow Over Rectangular-Prism Roughness Elements," J. Fluid Mech., **789**, pp. 127–165.
[29] Macdonald, R. W., Griffiths, R. F., and Hall, D. J., 1998, "An Improved Method for the Estimation of Surface Roughness of Obstacle Arrays," Atmos. Environ., **32**(11), pp. 1857–1864.
[30] Cionco, R., 1965, "A Mathematical Model for Air Flow in a Vegetative Canopy," J. Appl. Meteorol., **4**(4), pp. 517–522.
[31] Zhang, W., Zhu, X., Yang, X. I. A., and Wan, M., 2022, "Evidence for Raupach et al.'s Mixing-Layer Analogy in Deep Homogeneous Urban-Canopy Flows," J. Fluid Mech., **944**, p. A46.
[32] Raupach, M., 1992, "Drag and Drag Partition on Rough Surfaces," Boundary-Layer Meteorol., **60**(4), pp. 375–395.
[33] Schlichting, H., 1979, *Boundary-Layer Theory*, McGraw-Hill, New York.
[34] Jouybari, M. A., Yuan, J., Brereton, G. J., and Murillo, M. S., 2021, "Data-Driven Prediction of the Equivalent Sand-Grain Height in Rough-Wall Turbulent Flows," J. Fluid Mech., **912**, p. A8.
[35] Yuan, J., and Piomelli, U., 2014, "Estimation and Prediction of the Roughness Function on Realistic Surfaces," J. Turbul., **15**(6), pp. 350–365.
[36] Yang, J., Stroh, A., Chung, D., and Forooghi, P., 2022, "Direct Numerical Simulation-Based Characterization of Pseudo-Random Roughness in Minimal Channels," J. Fluid Mech., **941**, p. A47.
[37] Schultz, M. P., and Flack, K. A., 2007, "The Rough-Wall Turbulent Boundary Layer From the Hydraulically Smooth to the Fully Rough Regime," J. Fluid Mech., **580**, pp. 381–405.
[38] Thakkar, M., Busse, A., and Sandham, N., 2017, "Surface Correlations of Hydrodynamic Drag for Transitionally Rough Engineering Surfaces," J. Turbul., **18**(2), pp. 138–169.
[39] Yang, X. I. A., and Meneveau, C., 2017, "Modelling Turbulent Boundary Layer Flow Over Fractal-Like Multiscale Terrain Using Large-Eddy Simulations and Analytical Tools," Philos. Trans. R. Soc. A: Math., Phys. Eng. Sci., **375**(2091), p. 20160098.
[40] Medjnoun, T., Rodriguez-Lopez, E., Ferreira, M. A., Griffiths, T., Meyers, J., and Ganapathisubramani, B., 2021, "Turbulent Boundary-Layer Flow Over Regular Multiscale Roughness," J. Fluid Mech., **917**, p. A1.
[41] Womack, K. M., Volino, R. J., Meneveau, C., and Schultz, M. P., 2022, "Turbulent Boundary Layer Flow Over Regularly and Irregularly Arranged Truncated Cone Surfaces," J. Fluid Mech., **933**, p. A38.
[42] Xu, H. H., Altland, S. J., Yang, X. I., and Kunz, R. F., 2021, "Flow Over Closely Packed Cubical Roughness," J. Fluid Mech., **920**, p. A37.
[43] Yang, X., Xu, H., Huang, X., and Ge, M.-W., 2019, "Drag Forces on Sparsely Packed Cube Arrays," J. Fluid Mech., **880**, pp. 992–1019.